

Electron Acceleration in 3D Magnetic Reconnection with a Guide Field

J. T. Dahlin, J. F. Drake,* and M. Swisdak

*Institute for Research in Electronics and Applied Physics,
University of Maryland, College Park, Maryland 20742, USA*

(Dated: December 7, 2024)

Abstract

A kinetic simulation of 3D collisionless magnetic reconnection with a guide field shows a dramatic enhancement of electron acceleration when compared with a 2D system. In the 2D system, electrons are trapped in magnetic islands which limits their energy gain, whereas in the 3D system the filamentation of the current layer leads to a stochastic magnetic field that enables the electrons to access volume-filling acceleration regions. The dominant accelerator of the most energetic electrons is a Fermi-like mechanism associated with reflection of charged particles from contracting field lines.

Magnetic reconnection is a ubiquitous plasma process that converts magnetic energy into thermal and kinetic energy. Of particular interest is the production of non-thermal particles, in which a fraction of the plasma population is driven to energies much larger than that found in the ambient medium. Reconnection is thought to be an important driver of such particles in phenomena such as gamma ray bursts [1, 2], stellar and solar flares [3], and magnetospheric storms [4]. Recent observations of solar flares reveal the remarkable efficiency of electron acceleration: a large fraction of the electrons in the flaring region become a part of the nonthermal spectrum, with a resulting energy content comparable to that of the magnetic field [5, 6].

Mechanisms for particle acceleration have been explored and compared in a variety of papers, e.g. [7–13]. Several authors [9, 14, 15] have examined acceleration by electric fields parallel to the local magnetic field (E_{\parallel}). However, parallel electric fields are typically localized near reconnection X-lines and separatrices, which limits the number of electrons that can be accelerated through this mechanism.

Drake et al. [16] proposed a mechanism whereby charged particles gain energy as they reflect from the ends of contracting magnetic islands, a process analogous to the first-order Fermi acceleration of cosmic rays. This mechanism operates wherever there are contracting field lines in a reconnection region, and therefore develops during single X-line reconnection or as magnetic islands merge [12, 13, 16–18]. This mechanism is therefore volume filling and can accelerate a large number of particles.

In a recent article [19], we developed a method for calculating electron acceleration due to the three fundamental mechanisms: parallel electric fields E_{\parallel} , betatron acceleration associated with conservation of the magnetic moment, and Fermi reflection due to the relaxation of curved magnetic field lines. We found that Fermi reflection dominated in reconnection where the magnetic fields are roughly antiparallel (a result also found in [20]). However, in guide field reconnection, (in which the rotation angle of the magnetic field across the current layer is less than 180 degrees) where the current layers around the X-line and associated

regions where $E_{\parallel} \neq 0$ are longer, Fermi reflection and E_{\parallel} were both important drivers of particle acceleration. However, we did not address the scaling of each mechanism with particle energy. This is important for determining the mechanism responsible for producing the most energetic particles.

Studies of particle acceleration in reconnection have primarily been based on 2D simulations, in which accelerated particles are typically localized near the x-line, along magnetic separatrices and within magnetic islands [9, 20]. There are some observations with small ambient guide fields [21–23] that support such a picture. A notable exception are the Wind observations in which energetic electrons up to 300 keV are seen for more than an hour in an extended region around the reconnection region [4]. These observations corresponded to reconnection with a strong guide field.

Two-dimensional simulations impose limitations on the magnetic topology as well as the available spectrum of instabilities. In 3D reconnection without a guide field reconnection remains largely unchanged from 2D except for the development of interchange instabilities at the front of the outflow jet [24, 25]. In the presence of an ambient guide field, however, reconnection in 3D can become turbulent as a result of the generation of magnetic islands along separatrices and adjacent surfaces [26, 27]. While test particle trajectories in MHD fields have been used to explore acceleration in such systems, [28, 29] the absence of feedback of energetic particles on the reconnection process in such models limits their applicability to real systems. Recent 3D studies of kinetic reconnection examined particle acceleration in electron-positron plasmas [20, 30]. However, these studies focused on relativistic regimes where the magnetic energy per particle exceeds the rest mass energy and included no ambient guide field. Hence, the impact of complex 3D magnetic fields on particle acceleration remains an open topic.

Here, we explore magnetic reconnection in a 3D system with a strong guide field which is the most generic form of reconnection in space and astrophysical plasmas. We find that the efficiency of particle acceleration is greatly increased compared to that in a 2D system. We show that this occurs because the complex 3D magnetic fields enable the most energetic particles to access volume-filling acceleration sites rather than being confined to a single magnetic island which no longer accelerates particles once it has fully contracted. We also examine the energy dependence of the dominant E_{\parallel} and Fermi acceleration mechanisms, and find that Fermi reflection is the primary accelerator of the energetic electrons.

We explore particle acceleration via simulations using the massively parallel 3D particle-in-cell (PIC) code `p3d` [31]. Particle trajectories are calculated using the relativistic Newton-Lorentz equations, and the electromagnetic fields are advanced using Maxwell's equations. The simulations are initialized with a force-free magnetic field of the following form: $B_x = B_0 \tanh(y/w_0)$ and $B_z = \sqrt{2B_0^2 - B_x^2}$, where B_0 is the asymptotic value of B_x and $w_0 = 0.25d_i$. This geometry corresponds to an asymptotic guide field with a magnitude equal to B_0 . We include two current sheets at $y = L_y/4$ and $3L_y/4$ to produce a periodic system. The force-free configuration is chosen as the most generic model for large-scale systems such as the solar corona where the density jump between the current layer and the upstream plasma is not expected to be important.

The time and space coordinates are normalized, respectively, to the proton cyclotron time $\Omega_{ci}^{-1} = m_i c / eB$ and inertial length $d_i = c / \omega_{pi}$. We simulate a 3D domain with dimensions $L_x \times L_y \times L_z = 51.2d_i \times 25.6d_i \times 25.6d_i$ and an analogous 2D domain with $L_x \times L_y = 51.2d_i \times 25.6d_i$. The grid cell width is $d_e/4$, where $d_e = d_i \sqrt{m_e/m_i}$ is the electron inertial length. We use an artificial proton to electron mass ratio $m_i/m_e = 25$. The 3D simulation used 50 particles per cell for each species, and the 2D simulation used 1600 particles per cell. A 3D simulation with 100 particles per cell produced nearly identical results. The boundary conditions are periodic in all three dimensions, which are most relevant for a large current sheet with many interacting magnetic islands which is expected in large systems such as the solar corona [32, 33]. The time step is $dt = 0.01\Omega_{ci}^{-1} = 0.25\Omega_{ce}^{-1}$, where $\Omega_{ce} = (m_i/m_e)\Omega_{ci}$ is the electron cyclotron frequency. The initial electron and proton temperatures are $T_e = T_i = 0.25m_i c_A^2$, and the initial density n_0 and pressure p are constant so that $\beta = 8\pi p/B^2 = 0.5$. The speed of light is $c = 15c_A$, where $c_A = B_0/\sqrt{4\pi m_i n_0}$.

Reconnection develops from particle noise via the tearing instability, generating interacting flux ropes which grow and merge until they reach the system size at $t\Omega_{ci} \sim 50$. The macroscopic evolution of the 2D and 3D systems is similar at this point, though the 2D simulation has released roughly 15% more magnetic energy. Fig. 1 shows an isosurface of one component of the electron current density J_{ez} at $t\Omega_{ci} = 50$ in the 3D simulation. The current exhibits filamentary structure which develops from instabilities with $k_z \neq 0$ that are prohibited in 2D reconnection simulations [27].

Energy spectra (top panel of Fig. 2) reveal significant electron acceleration in both simulations. However, the 3D simulation produces a greater number of energetic particles:

the fraction of electrons with energy exceeding $0.5m_e c^2$ is roughly an order of magnitude larger than in the 2D simulation. Since the magnetic energy dissipation is greater in the 2D system, this suggests that the increased energetic electron production in the 3D system is due to enhanced acceleration efficiency rather than an increase in the total energy imparted to the plasma.

The spatial distribution of the most energetic particles (shown in the left-hand panels of Fig. 3) also differs between these simulations: these particles occupy narrow bands well inside the islands in the 2D simulation, but are distributed throughout the reconnecting region in the 3D simulation. In the 2D system, the reconnected field lines form closed loops (islands) that trap particles. The stochastic structure of the magnetic field in the 3D system, however, allows field-line-following particles to wander throughout the chaotic reconnecting region [34]. The distribution of the energetic particles in the 3D simulation is broadly consistent with Wind magnetotail observations where energetic electrons are seen for more than an hour and therefore must occupy a large region [4].

In order to examine the mechanisms responsible for accelerating these particles, we assume a guiding-center approximation relevant for a strong guide field [35]. In this limit, the evolution of the kinetic energy ϵ of a single electron can be written as:

$$\frac{d\epsilon}{dt} = qE_{\parallel}v_{\parallel} + \frac{\mu}{\gamma} \left(\frac{\partial B}{\partial t} + \mathbf{u}_E \cdot \nabla B \right) + \gamma m_e v_{\parallel}^2 (\mathbf{u}_E \cdot \boldsymbol{\kappa}) \quad (1)$$

where $E_{\parallel} = \mathbf{E} \cdot \mathbf{b}$ is the parallel electric field, $\mu = m_e \gamma^2 v_{\perp}^2 / 2B$ is the magnetic moment, \mathbf{u}_E is the $\mathbf{E} \times \mathbf{B}$ velocity corresponding to the advection of the magnetic field, and $\boldsymbol{\kappa} = \mathbf{b} \cdot \nabla \mathbf{b}$ is the magnetic curvature. The velocity components parallel and perpendicular to the magnetic field are v_{\parallel} and v_{\perp} , respectively; γ is the relativistic Lorentz factor, and \mathbf{b} is the unit vector in the direction of the local magnetic field.

The first term on the right-hand-side of the equation corresponds to acceleration by parallel electric fields, which are typically localized near the reconnection X-line and along separatrices. The second term corresponds to betatron acceleration and is a consequence of the conservation of the magnetic moment μ : when a particle experiences a change in B , its perpendicular energy evolves to compensate. In the case of reconnection, which reduces the overall magnetic field, betatron acceleration typically reduces particle energy [19]. The last term corresponds to reflection of particles from contracting magnetic field lines, a type of first order Fermi acceleration [13, 16, 17]. This occurs where tension is released as magnetic

fields advect in the direction of magnetic curvature ($\mathbf{u}_E \cdot \boldsymbol{\kappa} > 0$).

Equation 1 reveals that the acceleration mechanisms have different scaling with the particle energy: the Fermi reflection term is second order in the parallel velocity, whereas the parallel electric field term is only first order. The bottom panel of Fig. 2 shows the average acceleration per particle for both E_{\parallel} and Fermi reflection in the 3D simulation at $t\Omega_{ci} = 50$. The bulk thermal electrons (low energies) are primarily accelerated by E_{\parallel} , whereas Fermi reflection is more important at high energies. This indicates that Fermi reflection is the dominant accelerator of the most energetic particles, consistent with the energy scaling of Eq. 1.

The spatial distribution of the Fermi reflection term for the most energetic electrons ($> 0.5m_e c^2$) is shown on the right-hand side of Fig. 3. While acceleration occurs throughout the reconnection exhaust in the 3D simulation, in 2D the acceleration is limited to narrow bands near the cores of magnetic islands. This contrast suggests that the stochastic 3D field structure allows the electrons to have greater access to the acceleration regions where magnetic energy is being released.

To explore the reason for enhanced acceleration in the 3D system, we examine the trajectories of the 750 most energetic electrons in each simulation. A typical trajectory from the 2D simulation is shown in the top left panel in Fig. 4. The electron begins in the tail of the electron distribution with kinetic energy $\epsilon \approx 0.4m_e c^2$. The electron streams along a field line outside the reconnection region before accelerating at an X-line near $x \sim 50$ and becoming trapped in an island. The electron bounces several times inside this island, accelerating up to $\epsilon \approx 0.8m_e c^2$. By this point, the field line the electron is following has released its tension, so acceleration ceases even as the electron continues to bounce.

The top right panel of Fig. 4 shows a typical electron trajectory from the 3D simulation. The electron is not confined to a single island, but instead moves throughout the reconnecting domain. This allows it to undergo significantly greater acceleration than the electron from the 2D simulation, as it is able to return to active acceleration regions rather than being confined to the stagnant field lines near island cores. The acceleration of this particle is spread across a number of different islands, enabling it to reach a maximum energy of $\epsilon \approx 1.15m_e c^2$. The Supplemental Material [37] includes videos of both particle trajectories in the time evolving field of the simulation.

The electron trajectories shown here are relatively generic for their respective simulations.

Though the acceleration details differ, all of the electrons in the 2D simulation are confined to single islands, whereas no electrons in the 3D simulation show significant trapping. The bottom panels of Fig. 4 show the distribution of simulation $f(|\Delta x| = |x(\Omega_{ci}t = 50) - x(\Omega_{ci}t = 25)|)$ for the 750 most energetic particles in each simulation (the choice of $\Omega_{ci}t = 25$ as the earliest time eliminates free streaming along unreconnected field lines before islands develop). The average displacement of the energetic electrons in the 3D system is nearly an order of magnitude greater than that in the 2D simulation, underscoring a fundamental difference in the particle trajectories of the two systems.

It has been shown previously that the development of pressure anisotropy with $p_{\parallel} \gg p_{\perp}$ causes the cores of magnetic islands to approach firehose marginal stability, where the tension driving magnetic reconnection ceases, thereby throttling reconnection. A full treatment of the feedback from particle acceleration (e.g. [18]) is outside the scope of this paper. However, we do find that large anisotropies $p_{\parallel} > p_{\perp}$ persist in the 3D simulation, so the turbulent dynamics do not appear to significantly isotropize the pressure. It therefore seems likely that energetic particle feedback on reconnection through the firehose mechanism will continue in the more complex magnetic geometry of 3D systems.

The electron spectra in both simulations do not assume a power law form as is frequently observed in nature. This is due in part to the limited energy gain possible in the modest-sized 3D simulation presented here. Previous 2D simulations have shown the total energy gain is greater in larger systems [19]. An additional issue is that these simulations have periodic boundary conditions so no particles are lost from the system. Solar observations suggest that electrons are confined in regions of energy release in the corona [5]. The mechanism for confinement remains an open issue. Both magnetic mirroring and double layers are possible mechanisms [36]. On the other hand, it has been suggested that the development of a power law requires a loss mechanism in addition to an energy drive [18]. However, recent electron-positron simulations [20, 30] suggest that power law spectra may still develop in the absence of a loss mechanism. The set of conditions under which power law spectra form in kinetic reconnection simulations remains an open issue.

A limitation of the present simulations is the use of an artificial mass ratio which reduces the separation between proton and electron scales. In order for an electron to access multiple acceleration sites as we observe in our simulations, its characteristic velocity must exceed that of the macroscopic flows associated with the protons. This suggests that we have

achieved a significant separation of scales; by comparison, proton spectra (not shown) do not exhibit enhanced acceleration in the 3D system. The absence of such a separation of scales may explain why this behavior is not observed in electron-positron simulations [20].

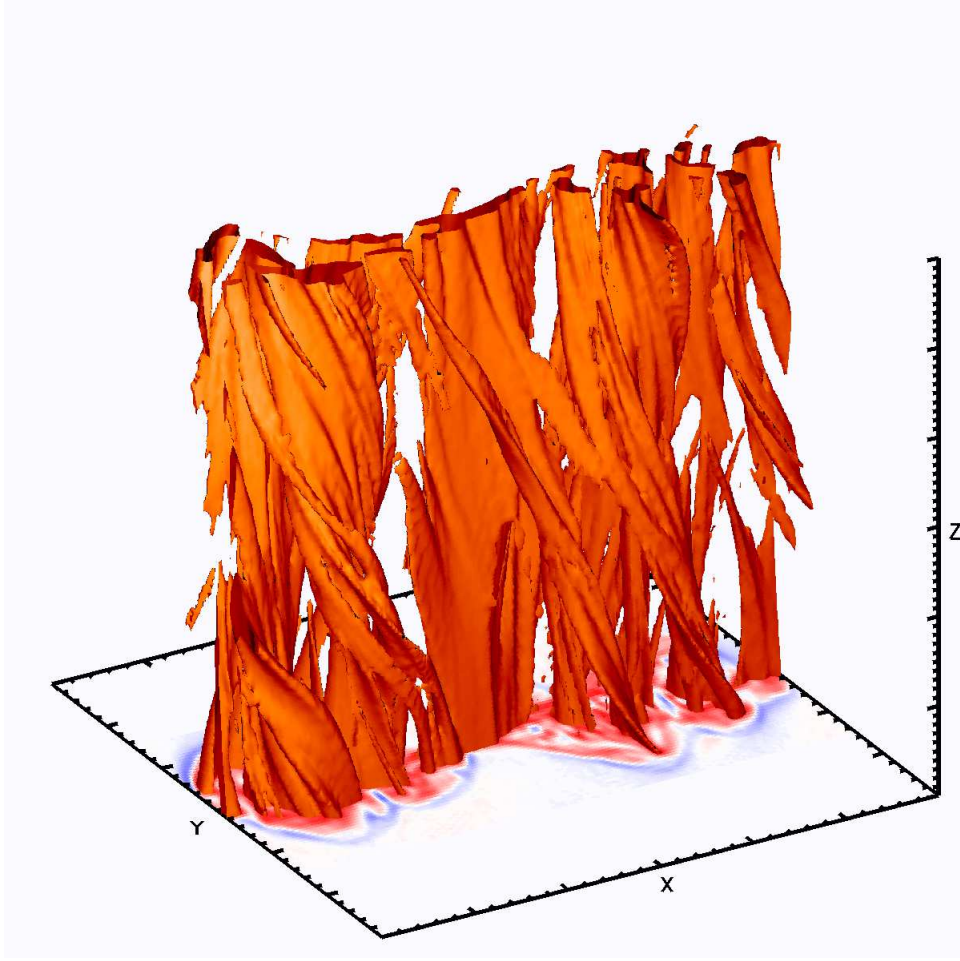


FIG. 1. Isosurface of J_{ez} at $t\Omega_{ci} = 50$. The isosurface level is 60% of the maximum current density (a 2D slice of the same quantity is shown on the bottom). The current is filamentary, exhibiting significant 3D structure.

This work has been supported by NSF Grants AGS1202330 and PHY1102479, and NASA grants NNX11AQ93H, APL-975268, NNX08AV87G, NAS 5- 98033, and NNX08AO83G. Simulations were carried out at the National Energy Research Scientific Computing Center.

* Department of Physics, University of Maryland, College Park, Maryland 20742, USA; Institute for Physical Science and Technology, University of Maryland, College Park, Maryland 20742, USA; Space Science Laboratory, University of California, Berkeley, California 94720, USA

[1] G. Drenkhahn and H. C. Spruit, *Astronomy & Astrophysics* **391**, 1141 (2002).

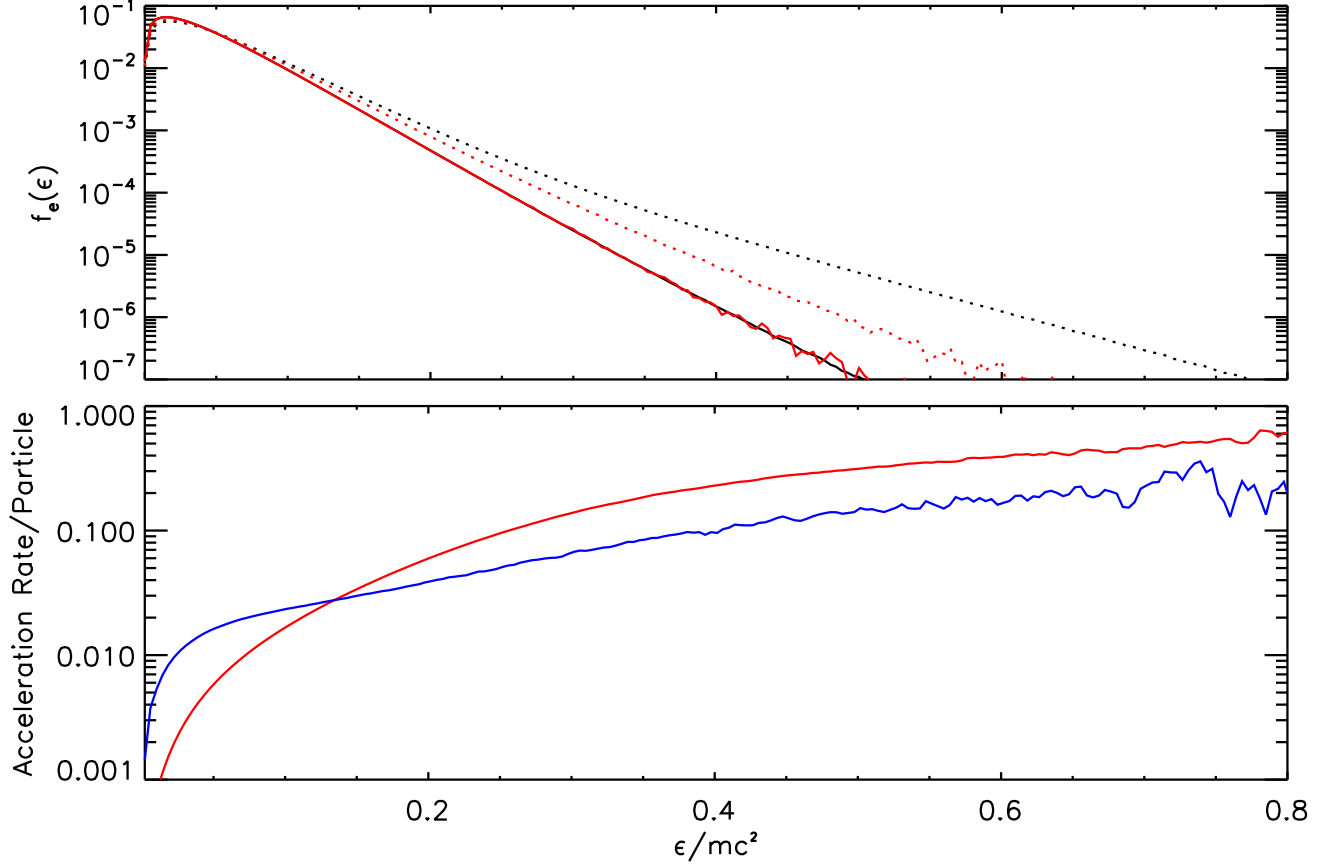


FIG. 2. [Top] Global electron energy spectra at the beginning (solid lines) and end (dotted lines) of 2D (red) and 3D (black) simulations. The energetic electrons in the 3D simulation gain significantly more energy. [Bottom] Acceleration due to E_{\parallel} (blue) and Fermi Reflection (red) in the 3D simulation at $t\Omega_{ci} = 50$. Parallel electric fields are most important for low energies, whereas Fermi reflection dominates at high energies.

[2] F. C. Michel, *Ap. J.* **431**, 397 (1994).

[3] R. P. Lin, S. Krucker, G. J. Hurford, D. M. Smith, H. S. Hudson, G. D. Holman, R. A. Schwartz, B. R. Dennis, G. H. Share, R. J. Murphy, A. G. Emslie, C. Johns-Krull, and N. Vilmer, *Ap. J.* **595**, L69 (2003).

[4] M. Øieroset, R. P. Lin, T. D. Phan, D. E. Larson, and S. D. Bale, *Phys. Rev. Lett.* **89**, 195001 (2002).

[5] S. Krucker, H. S. Hudson, L. Glesener, S. M. White, S. Masuda, J.-P. Wuelser, and R. P. Lin, *Ap. J.* **714**, 1108 (2010).

[6] M. Oka, S. Ishikawa, P. Saint-Hilaire, S. Krucker, and R. P. Lin,

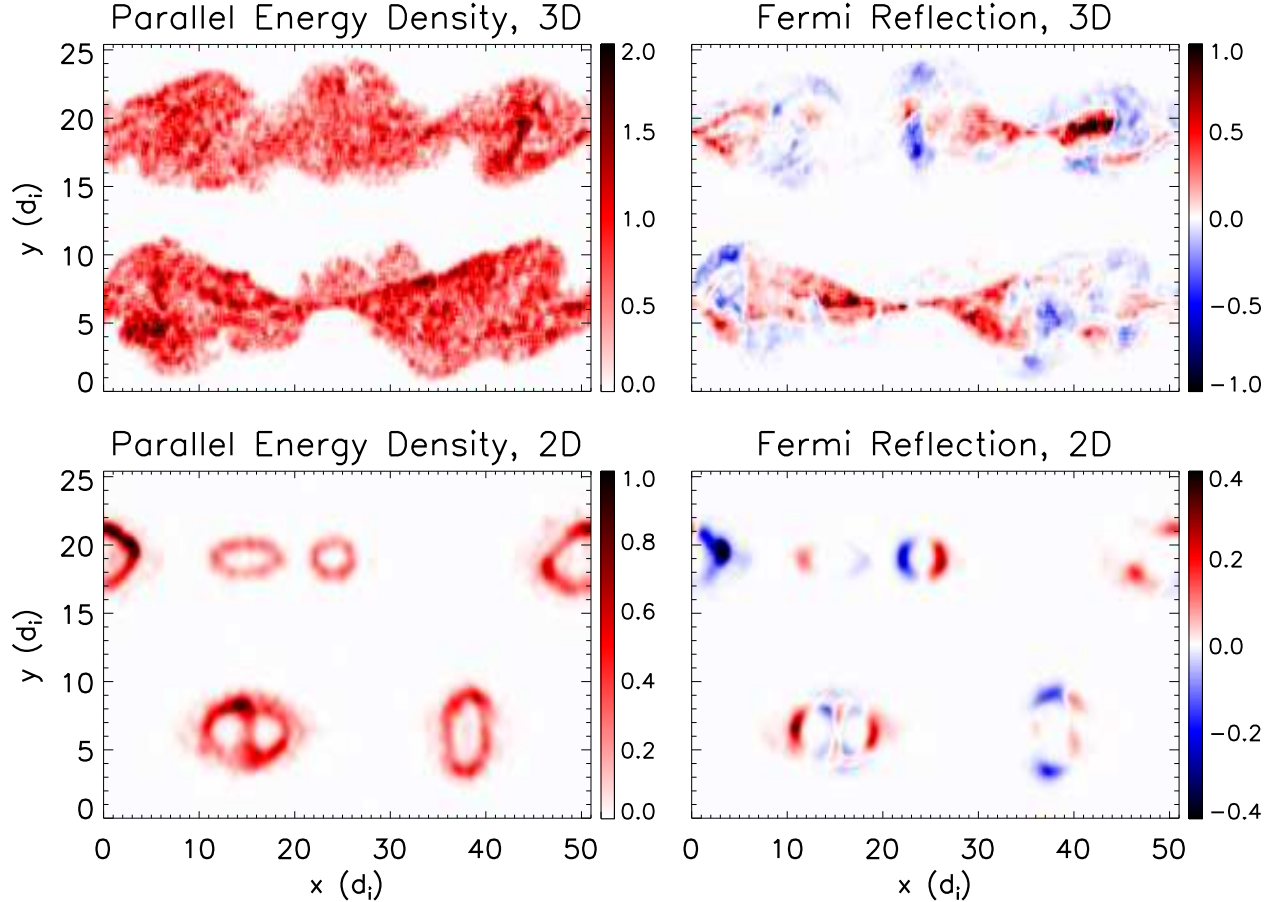


FIG. 3. Parallel energy density and Fermi reflection heating rate for electrons with $\epsilon > 0.5m_e c^2$ in the plane $z = 0$ at $\Omega_{ci}t = 50$. The energetic particles are confined to narrow rings in the 2D simulation, but are distributed throughout the reconnecting volume in the 3D simulation. This is reflected in the Fermi reflection heating rate, which is also localized to the rings in the 2D simulation, but distributed throughout the reconnection exhaust in the 3D simulation.

The Astrophysical Journal **764**, 6 (2013).

- [7] M. Hoshino, T. Mukai, T. Terasawa, and I. Shinohara, J. Geophys. Res. **106**, 25,979 (2001).
- [8] S. Zenitani and M. Hoshino, Ap. J. Lett. **562**, L63 (2001).
- [9] J. F. Drake, M. A. Shay, W. Thongthai, and M. Swisdak, Phys. Rev. Lett. **94**, 095001 (2005).
- [10] P. L. Pritchett, J. Geophys. Res. **111**, A10212 (2006), 10.1029/2006JA011793.
- [11] J. Egedal, W. Daughton, J. F. Drake, N. Katz, and A. Lê, Phys. Plasmas **16**, 050701 (2009), 10.1063/1.3130732.
- [12] M. Oka, T.-D. Phan, S. Krucker, M. Fujimoto, and I. Shinohara, Ap. J. **714**, 915 (2010).
- [13] M. Hoshino, Phys. Rev. Lett. **108**, 135003 (2012).

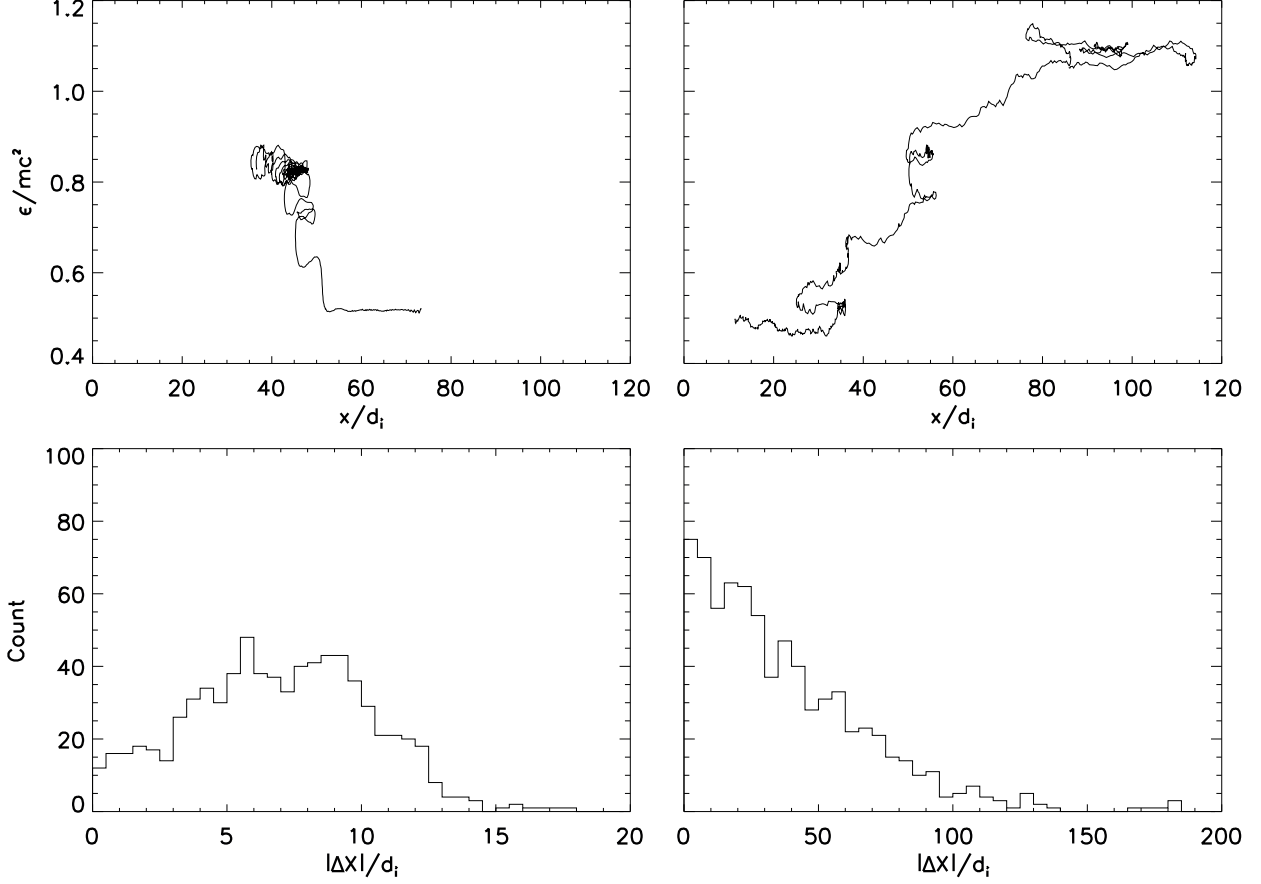


FIG. 4. [Top] Typical energy vs. position plots for an energetic particle in the 2D system (left) and the 3D system (right) over the period $\Omega_{ci}t = 0$ to 50. The electron in the 3D simulation continuously gains energy as it moves throughout the domain. The electron in the 2D simulation is trapped in an island at $x \sim 40$ for a significant period of time and no longer gains energy after the island has released its tension. [Bottom] Distribution of $\Delta X = |x(t = 50) - x(t = 25)|$ for the 750 most energetic particles in the 2D simulation (left) and 3D simulation (right). The particles in the 3D simulation are able to access a much larger fraction of the simulation domain.

[14] Y. E. Litvinenko, *Ap. J.* **462**, 997 (1996).

[15] J. Egedal, W. Daughton, and A. Lê, *Nature Phys.* **8**, 321 (2012).

[16] J. F. Drake, M. Swisdak, H. Che, and M. A. Shay, *Nature* **443**, 553 (2006).

[17] J. F. Drake, M. Opher, M. Swisdak, and J. N. Chamoun, *Ap. J.* **709**, 963 (2010).

[18] J. F. Drake, M. Swisdak, and R. Fermo, *The Astrophysical Journal Letters* **763**, L5 (2013).

[19] J. T. Dahlin, J. F. Drake, and M. Swisdak, *Physics of Plasmas (1994-present)* **21**, 092304 (2014).

[20] F. Guo, H. Li, W. Daughton, and Y.-H. Liu, *Phys. Rev. Lett.* **113**, 155005 (2014).

- [21] L.-J. Chen, A. Bhattacharjee, P. A. Puhl-Quinn, H. Yang, N. Bessho, S. Imada, S. Mühlbacher, P. W. Daly, B. Lefebvre, Y. Khotyaintsev, A. Vaivads, A. Fazakerley, and E. Georgescu, *Nature Physics* **4**, 19 (2007).
- [22] A. Retin, R. Nakamura, A. Vaivads, Y. Khotyaintsev, T. Hayakawa, K. Tanaka, S. Kasahara, M. Fujimoto, I. Shinohara, J. P. Eastwood, M. Andr, W. Baumjohann, P. W. Daly, E. A. Kronberg, and N. Cornilleau-Wehrin, *Journal of Geophysical Research: Space Physics* **113** (2008), 10.1029/2008JA013511, a12215.
- [23] S. Y. Huang, A. Vaivads, Y. V. Khotyaintsev, M. Zhou, H. S. Fu, A. Retin, X. H. Deng, M. Andr, C. M. Cully, J. S. He, F. Sahraoui, Z. G. Yuan, and Y. Pang, *Geophysical Research Letters* **39**, n/a (2012), 111103.
- [24] P. L. Pritchett, *J. Geophys. Res.* **106**, 25961 (2001).
- [25] M. S. Nakamura, H. Matsumoto, and M. Fujimoto, *Geophysical Research Letters* **29**, 88 (2002).
- [26] R. Schreier, M. Swisdak, J. F. Drake, and P. A. Cassak, *Phys. Plasmas* **17**, 110704 (2010), 10.1063/1.3494218.
- [27] W. Daughton, V. Roytershteyn, H. Karimabadi, L. Yin, B. J. Albright, B. Bergen, and K. J. Bowers, *Nature Phys.* **7**, 539 (2011).
- [28] M. Onofri, H. Isliker, and L. Vlahos, *Phys. Rev. Lett.* **96**, 151102 (2006), 10.1103/PhysRevLett96.151102.
- [29] G. Kowal, E. M. de Gouveia Dal Pino, and A. Lazarian, *The Astrophysical Journal* **735**, 102 (2011).
- [30] L. Sironi and A. Spitkovsky, *The Astrophysical Journal Letters* **783**, L21 (2014).
- [31] A. Zeiler, D. Biskamp, J. F. Drake, B. N. Rogers, M. A. Shay, and M. Scholer, *J. Geophys. Res.* **107**, 1230 (2002).
- [32] P. A. Cassak, M. A. Shay, and J. F. Drake, *Phys. Plasmas* **16**, 120702 (2009), 10.1063/1.3274462.
- [33] Y.-M. Huang and A. Bhattacharjee, *Phys. Plasmas* **17**, 062104 (2010), 10.1063/1.3420208.
- [34] J. R. Jokipii and E. N. Parker, *Astrophys. J.* **155**, 777 (1969).
- [35] T. G. Northrop, “The adiabatic motion of charged particles,” (Interscience Publishers, 1963).
- [36] T. C. Li, J. F. Drake, and M. Swisdak, *The Astrophysical Journal* **757**, 20 (2012).
- [37] See Supplemental Material at [URL] for .mov movies of the particle trajectories .